Nanotechnology **20** (2009) 405203 (5pp) doi:10.1088/0957-4484/20/40/405203

The effect of next nearest neighbor coupling on the optical spectra in bilayer graphene

A R Wright[1], Feng Liu[2] and C Zhang[1]

[1] School of Engineering Physics, University of Wollongong, New South Wales 2552, Australia
[2] Department of Materials Science and Engineering, University of Utah, Salt Lake City, UT 84112, USA

Received 2 July 2009, in final form 17 August 2009
Published 8 September 2009
Online at stacks.iop.org/Nano/20/405203

Abstract
We investigate the dependence of the optical conductivity of bilayer graphene (BLG) on the intra and interlayer interactions using the most complete model to date. We show that the next nearest neighbor intralayer coupling introduces new features in the low energy spectrum significantly changing the 'universal' conductance. Further, its interplay with interlayer couplings leads to an anisotropy in the conductance in the ultraviolet range. We propose that experimental measurement of the optical conductivity of intrinsic and doped BLG will provide a good benchmark for the relative importance of intra and interlayer couplings at different doping levels.

(Some figures in this article are in colour only in the electronic version)

Since the isolation of single layers of graphite in 2003 [1], a lot of exciting work on single layer graphene (SLG) has been done [2]. For example, the prediction and observation of electron–hole symmetry and a half-integer quantum Hall effect [3–5], finite conductivity at zero charge-carrier concentration [3], the strong suppression of weak localization [6–8], universal conductance [9–11], magnetic enhancement of optical conductance in graphene nanoribbons [12] and a strong nonlinear response in the terahertz frequency regime [13, 14].

More recently, attention has also been paid to SLG's cousin, bilayer graphene (BLG). Electrons in bilayers can qualitatively exhibit new properties to those in single layers, such as interlayer drag [15] and correlation [16]. The electronic and transport properties of BLG differ significantly from SLG in many respects, particularly at low energies in the 'Dirac' regime. Various models for low energy BLG exist in the literature depending on the coupling terms included, and whether electronic bands beyond the lowest energy subbands are retained [17, 18]. Many interesting results were obtained based on a model that includes only the most dominant of the interlayer coupling terms in BLG, as well as the usual nearest neighbor intralayer term [19]. By including the second most dominant interlayer coupling, some unusual properties such as a peculiar Landau-level spectrum have been derived [18], as well as a new low energy peak in the optical conductance [20, 21]. By further increasing the layer numbers, one has graphene multilayers whose energy dispersion near the K-point can be tuned by a gate voltage [22].

The 'universal conductance' of graphene is both a dc and an ac phenomenon. It is a direct result of the linear energy dispersion of graphene. Linear subbands imply both a constant density of states as well as consistent transition matrix elements, which means that as long as the linear (Dirac) approximation is valid, the conductance is a constant. In the ac case, the value of the universal conductance of single layer graphene is $\sigma_1 = e^2/4\hbar$. In the layered case, a standard benchmark is simply $\sigma_n = n\sigma_1$. However, this is not generally accurate, as the subband curvature caused by interlayer coupling in the case of layered graphene leads to a non-constant conductivity. This raises an important question: in what energy range is $\sigma_n = n\sigma_1$ applicable?

The infrared conductance of BLG has been measured by several groups [23, 24]. These results rely upon the effects of an induced gate voltage on the bandstructure, which causes a difference in onsite energy between the two layers. In [22], Mak *et al* present the 'expected' IR conductance without the latter assumption, and find that it differs markedly from their experimental results. This demonstrates the need to assume an energetic discrepancy between the two layers in BLG. Our theoretical results, however, show a strong correlation to the results in [21] and [22], demonstrating that while an energetic

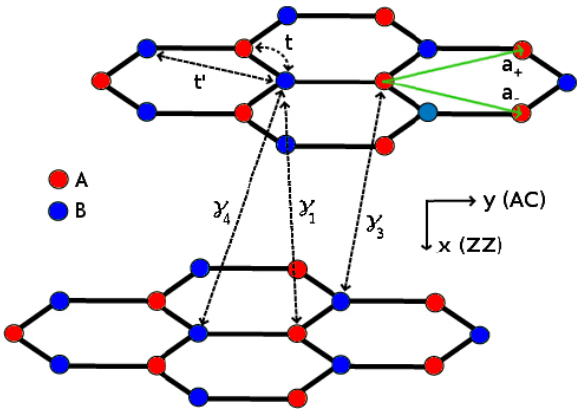

Figure 1. The three interlayer and two intralayer coupling terms included in the BLG Hamiltonian. γ_3 and γ_4 differ in that they connect, respectively, inequivalent (e.g. A–B) and equivalent (e.g. A–A) points in the SLG Brillouin zone. γ_1 is a directly vertical transition, and so the overlap of the wavefunctions is about 3× larger than γ_3 and γ_4. The armchair (AC) direction is given by the y-axis, and the zig-zag (ZZ) direction is given by the x-axis. The lattice vectors $\mathbf{a}_+$ and $\mathbf{a}_-$ are also shown.

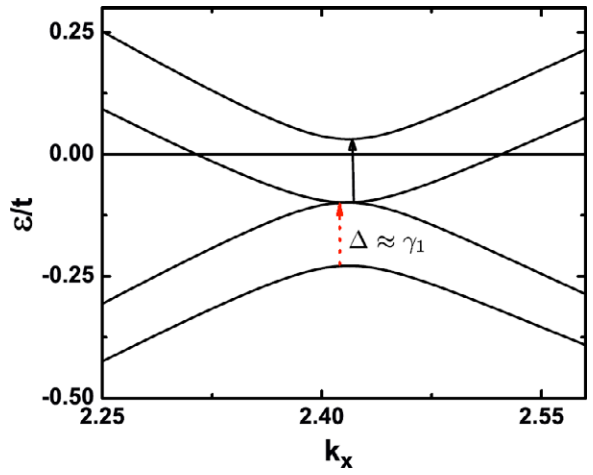

Figure 2. The k_x dependence of the bandstructure near the K/K′ points. The effect of the NNN coupling is to shift the Fermi level (here $\epsilon_F = 0$) off the bands-crossing points. The other noticeable effect here is that of the dominant interlayer coupling γ_1 which causes the gap of $\Delta \approx \gamma_1$ between similar bands. The red dashed arrow represents a transition which is permitted in an intrinsic bilayer calculation if NNN coupling is neglected in the model, but becomes forbidden when it is included. The black solid arrow is the opposite: a previously forbidden transition becomes allowed when NNNs are included in the model. The effect of doping is to raise or lower the Fermi level, making the inclusion of NNNs partly equivalent to doping.

discrepancy may exist, it is not necessary in describing the IR response observed experimentally.

In this paper, we study the dependence of the optical conductance of BLG on various intra and interlayer couplings. It is shown that the interplay of these couplings leads to a significant deviation in the behavior of the conductance at low frequencies, which can, in turn, be tuned by electronic doping. For this reason we will consider two important samples: intrinsic (i.e. undoped and unbiased) bilayer graphene, as well as a sample which is doped so as to drag the chemical potential to the bands-crossing point (see figure 2). In the important ultraviolet frequency band, this interplay leads to significant conductance anisotropy, i.e., the absorption along the zig-zag direction is around 50% stronger than that along the armchair direction.

A typical BLG sheet consists of two SLG layers stacked in the orientation shown in figure 1. Several forms of the Hamiltonian for BLG are used in the literature depending on the approximations used and the relative orientations of the two layers. The original consideration was given by Slonczewski–Weiss–McClure which included all three interlayer coupling terms [25, 26]. The most prominent interlayer term is the A–B and B–A coupling between sites which are directly above (or below) each other. Here we define this term as $\gamma_1 = 0.36$ eV. The other two interlayer coupling terms are the A–B and B–A coupling between inequivalent sites which are not directly above or below each other, but offset by an amount $b = 1.42$ Å, and the A–A and B–B terms which are similarly offset from one another, but represent equivalent sites in the SLG Brillouin zone. These coupling terms are defined here as $\gamma_3 = 0.10$ eV and $\gamma_4 = 0.12$ eV, respectively. We have also included the next nearest neighbor A–A and B–B coupling which we define as $t' = 0.10$ eV. Finally, as usual, the nearest neighbor A–B and B–A coupling is included, which is given here by $t = 3.0$ eV. All energies will be normalized relative to the nearest neighbor coupling term t.

The full Hamiltonian matrix for the BLG system is

$$H_{\mathrm{BLG}} = \begin{pmatrix} t'H' & tH^* & \gamma_4 H & \gamma_1 \\ tH & t'H' & \gamma_3 H^* & \gamma_4 H \\ \gamma_4 H^* & \gamma_3 H & t'H' & tH^* \\ \gamma_1 & \gamma_4 H^* & tH & t'H' \end{pmatrix}, \tag{1}$$

where $H = \mathrm{e}^{\mathrm{i}k_y a/\sqrt{3}}(1 + \mathrm{e}^{\mathrm{i}\mathbf{k}\cdot\mathbf{a}_+} + \mathrm{e}^{\mathrm{i}\mathbf{k}\cdot\mathbf{a}_-})$ and $H' = 2(\cos(\mathbf{k}\cdot\mathbf{a}_+) + \cos(\mathbf{k}\cdot\mathbf{a}_-) + \cos(\mathbf{k}\cdot(\mathbf{a}_+ - \mathbf{a}_-)))$. Here $\mathbf{a}_\pm = a(\pm\frac{1}{2}, \frac{\sqrt{3}}{2})$ are the two lattice vectors shown in figure 1. The eigenvalues and eigenvectors in the absence of γ_4 are readily solved. With γ_4 included, however, the form of the solution is unwieldy. The eigenvalues in the simpler case are given by the (relatively) concise form

$$\epsilon_{s,s'} = t'(\epsilon_{\mathrm{SLG}}^2 - 3) + s\sqrt{\epsilon_{\mathrm{SL}}^2 + \frac{\gamma_{12}^+}{2} + s'\sqrt{\Gamma}} \tag{2}$$

where

$$\Gamma = \epsilon_{\mathrm{SL}}^2 \gamma_{12}^+ + \frac{(\gamma_{12}^-)^2}{4} + 2\gamma_1\gamma_3\epsilon_{\mathrm{SL}}^2 \mathrm{Re}(H). \tag{3}$$

Also $\gamma_{12}^\pm = \gamma_3^2\epsilon_{\mathrm{SL}}^2 \pm \gamma_1^2$, with $s, s' = \pm 1$, and ϵ_{SL} are the regular eigenvalues for the SLG system given as

$$\epsilon_{\mathrm{SLG}} = t(1 + 4\cos(ak_x/2)\cos(ak_y/2\sqrt{3}) + 4\cos^2(ak_x/3))^{\frac{1}{2}}. \tag{4}$$

From this result we see that there are two conduction bands and two valence bands which are confined above and below the line $\epsilon_{s,s'} - t'(\epsilon_{\mathrm{SLG}}^2 - 3) \approx 3t'$ near the K points. This simple result will form the basis for much of the discussion to follow.

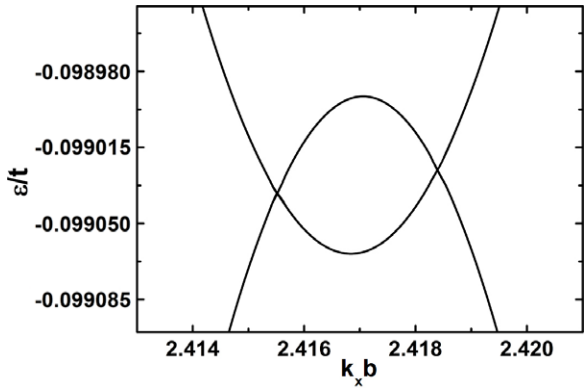

Figure 3. The k_x dependence of the two inner bands near the K/K′ points zoomed in to see the effects of the intralayer next nearest neighbors (NNN), and interlayer coupling terms γ_3 and γ_4. The NNN interaction has shifted these features well below the Fermi level. γ_3 causes a second Dirac point to emerge, and γ_4 skews the bandstructure, causing one of the two Dirac points to be pushed down to a lower energy.

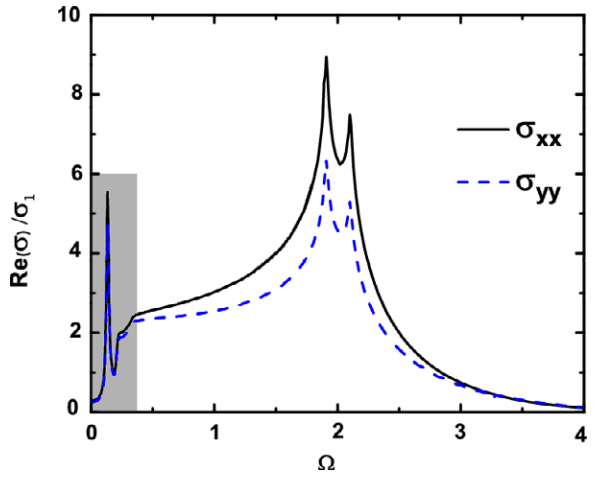

Figure 4. The optical conductance (in units of $\sigma_1 = e^2/\hbar$) versus the normalized frequency $\Omega = \hbar\omega/t$ for bilayer graphene. Generally, σ_{xx} (the zig-zag direction) has a larger optical response than σ_{yy} (the armchair direction). When NNN and γ_4 are neglected, and at low energies, $\sigma_{xx} = \sigma_{yy}$. This is no longer the case here, with NNNs and γ_4 included. The gray shaded area indicates the low energy region plotted in figure 5.

The electron field operators can be constructed from the eigenvectors $\psi_{s,s'}(\mathbf{k})$ such that $\Psi(\mathbf{r}) = (1/4\pi^2)\sum_{\mathbf{k},s,s'} a_{s,s'}(\mathbf{k})\psi_{s,s'}(\mathbf{k})e^{i\mathbf{k}\cdot\mathbf{r}}$, where $a_{s,s'}(\mathbf{k})(a^{\dagger}_{s,s'}(\mathbf{k}))$ denotes the annihilation (creation) operator for an electron in the s or s' subband with momentum $\mathbf{k}$.

The band structure of BLG near the K points varies dramatically depending on the coupling terms included in the Hamiltonian. The effect of the various coupling terms are as follows.

The next nearest neighbor term t' breaks the electron hole symmetry. The effect is small at low energies, but becomes significant at higher energies. In particular, the NNN induced anisotropy shifts the Fermi energy away from the bands-crossing points. This makes the lower conduction band fill at sufficiently low energies, drastically altering the behavior of interband-transition-dependent properties. The shift of the Fermi energy relative to the bands-crossing points can be seen in figure 2 where $\epsilon = 0$ corresponds to the Fermi energy.

The term γ_1 represents the dominant interlayer A–B and B–A coupling. This term causes an energy gap to form between the two conduction bands, and an identical gap between the two valence bands of $\gamma_1/t \approx 0.13$. γ_1 also removes the linear dispersion at low energies. The electron hole symmetry is retained, and no lateral warping occurs. The effect of γ_1 is apparent in figure 2.

The second interlayer coupling term γ_3 restores the linear lowest energy subband. This term causes what is usually referred to as 'trigonal warping' [18, 28]. A second set of Dirac points near the K/K′ points emerges with γ_3 included, as can be seen in figure 3.

Finally, γ_4 causes one of the Dirac points to be plunged below the NNN line, also seen in figure 3. When the next nearest neighbor term couples with γ_4, however, the low energy x–y isotropy is substantially weakened. While γ_3 causes the well known anisotropic 'trigonal warping', the energy range of this effect is in the order of $t/10\,000 \approx 0.0003$ eV. On its own, the effect of γ_4 is similarly small. Here, however, γ_4 and t' both couple equivalent sites, which causes a compounding of their individual effects on the electronic dispersion relation. The effect is quite a large deviation from isotropy. The effect of this deviation is most noticeable in the low energy conductance anisotropy shown in figure 5.

We now evaluate the optical conductivity of BLG in the absence of disorder or impurities, over all relevant photon energies. By using the Kubo formula, the optical conductivity is given as [29],

$$\sigma_{\mu,\nu}(\omega) = \frac{1}{\omega}\int_0^{\infty} \mathrm{d}t\, e^{i\omega t}\langle[J_\mu(t), J_\nu(0)]\rangle. \qquad (5)$$

The components of the current operator can be calculated from $J_{\nu,\mu}(t) = e^{iHt}J_{\nu,\mu}(0)e^{-iHt}$, where $J_{\nu,\mu}(0) = \Psi^{\dagger}(\mathbf{r})\hat{v}_{\nu,\mu}\Psi(\mathbf{r}')$, in which $\hat{v}_{\nu,\mu} = \partial H/\partial k_{\nu,\mu}$, and $\nu, \mu = x, y$. These values are calculated numerically, but we note that for each band there are three types of interband transitions, and also intraband transitions. In the case of no disorder and no intermediate interactions, it is found that intraband transitions cannot occur.

In figure 4 we examine the optical conductance of intrinsic bilayer graphene. Near the higher energy valley points, the optical conductance exhibits two extrema, similar to the single peak found in single layer graphene [27, 30]. These peaks correspond to the two dominant vertical transitions between the two symmetric pairs of saddle points. The joint density of states in these valleys reaches a cusp-like maximum which leads to the extrema in the conductance. These two energy peaks are separated by an amount $\hbar\omega = 2\gamma_1$, as expected from the bandstructure calculations. Finally note that the conductance along the zig-zag direction is generally larger than that along the armchair direction, especially at larger energies.

Figure 5 shows the low energy optical conductivity of the intrinsic sample from the gray shaded region of figure 4, as well as a sample doped to shift the Fermi level to the bands-crossing point. The longitudinal conductance varies greatly when including a non-zero NNN interaction in the

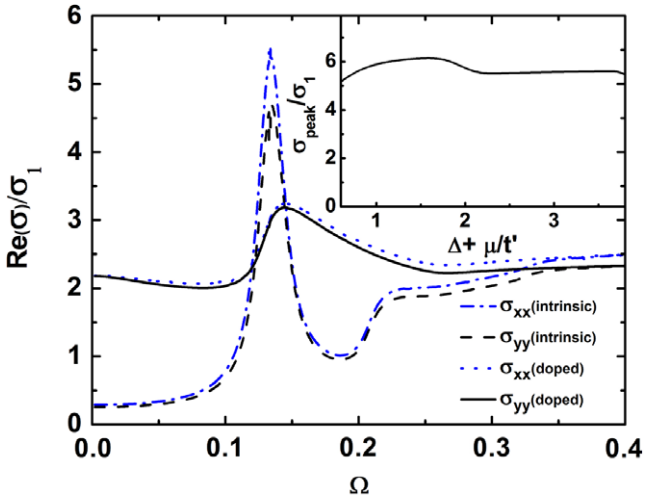

Figure 5. The low energy optical conductance at two different doping levels. The blue dash–dot and black dashed lines are the optical conductance of intrinsic BLG along the x and y directions respectively. The black solid and blue dotted lines represent the optical conductance of a sample which is doped such that the chemical potential is shifted to the bands-crossing point. The NNN–γ_4 coupling causes a new peak to emerge, and suppresses the previously reported one. This new peak is much larger and shifted to a lower photon energy. In a suitably doped sample, however, the $t' = 0$ (no NNN) peak has been retrieved by an effective shifting of the Fermi level. The inset shows the sensitivity of the intrinsic zig-zag peak to the Fermi energy. Δ is the bands-crossing point. If the Fermi energy lies at least $0.6t'$ from the bands-crossing points (in either direction), the peak conductance lies within about 10% of our result.

model, and the effect is equivalent to doping when NNN interactions are included. The effect of the dominant interlayer term γ_1 (i.e. setting $\gamma_3 = \gamma_4 = t' = 0$) at low energies has been reported recently [20]. This result has been retrieved in our NNN inclusive result by doping the sample so as to force the Fermi energy to coincide with the bands-crossing points. In the intrinsic case, however, the previously reported result is entirely suppressed, and replaced by an approximately $2\times$ larger, rounded peak, followed by a significant trough. This correlates well with the behavior observed in IR experiments [23, 24], although without the added effects of an induced gate voltage. In the doped sample, electron transitions from either valence band into either conduction band are allowed, which is equivalent to intrinsic bilayer graphene calculations with NNN coupling neglected, as shown in figure 2. The intrinsic bilayer sample with NNN interactions included in the model, however, suppresses transitions from the upper valence band to the lower conduction band, since they are both filled, and yet a new set of transitions become allowed between the two conduction bands. These similar bands are separated by an approximately constant factor of γ_1, which leads to the large peak centered at $\hbar\omega \approx \gamma_1$ in the intrinsic bilayer sample. The feature is in striking contrast with that of SLG. For SLG, the effect of the NNN coupling is to suppress the universal conductance at low frequencies [30]. As is clearly seen in figure 5, for BLG the interplay of the interlayer coupling and the NNN coupling can suppress the conductance at low frequencies. However, it also induces a strong absorption peak in the far infrared before the onset of the universal conductance.

For this reason, the low energy approximations of the behavior of bilayer graphene are generally more relevant to carefully doped samples, with the intrinsic bilayer properties being drastically affected by the next nearest neighbor hopping and additional interlayer terms. Whilst the existing low energy formalisms are capable of accurately reproducing the low energy bandstructures with these terms, in intrinsic bilayer graphene those bands will be completely filled, and predicted effects will be suppressed. In order to empty one of the two inner bands, the system must be doped (or biased) in some way, and to a very specific level. Furthermore, when using existing theories to explain experimental results, it needs to be noted that an energetic discrepancy between layers, as well as the inclusion of a gate voltage, both cause some similar effects to the inclusion of the NNN interaction. All of these will therefore need to be accounted for when explaining any experimental result.

Furthermore, the conductance anisotropy observed in figures 4 and 5, which is prominent even in the IR region when γ_4 and t' are both included, makes the polarization of the photon beam in experiments a relevant parameter. This orientation dependence of the optical conductance makes determination of the orientation of a BLG flake possible, and also makes BLG a potential partial polarizer. The doping dependence of the low energy conductance anisotropy makes this feature quite versatile. We note, however, that this anisotropy is stronger when the chemical potential lies above the Fermi level than when it is below it. This partly explains the effect noticed by Li *et al* [23] which is that the bias of the gate voltage breaks electron–hole symmetry.

Finally, as we have already mentioned, the value of the 'universal' conductivity is a topic of great interest at the moment. According to these results, which have been calculated from the most robust interlayer and intralayer model adopted to date, the value of the universal conductivity for bilayer graphene is $\sigma_2 = 2\sigma_1$ where $\sigma_1 = e^2/4\hbar$ is the universal optical conductivity of single layer graphene defined earlier. The range over which this value is applicable is greatly affected by the inclusion of the NNN interaction in numerical calculations, and is strongly dependent on the electronic doping of a real sample. In particular, the NNN interaction causes the very low energy optical response to become negligible, and around the observed peak, the optical conductance is $\sigma_{\text{peak}} \approx 5.6\sigma_1$.

From our results, it is clear that the universal conductivity is an approximation that applies only within certain energy ranges and is strongly dependent on sample doping. For intrinsic BLG, the energy ranges where $\sigma_2 \approx 2\sigma_1$ is $\hbar\omega > 0.4t$. However, this quickly becomes inaccurate with increasing energy, especially for σ_{xx}. For a doped sample however, the approximation can be much more appropriate. In this case the applicable energy ranges are $\hbar\omega < 0.13t$, and $\hbar\omega > 0.25t$.

Before concluding, we mention in passing that the exact location of the Fermi energy is not widely agreed upon as its determination involves many factors. In this work we choose the natural $\epsilon = 0$ point that arises from the tight-binding formalism adopted. This choice is somewhat arbitrary.

The breaking of electron hole symmetry induced by NNN interactions assures that the Fermi energy will not coincide with the bands-crossing points by at least an amount of the order of t'. For Fermi energies above or below the neighborhood of these points, the low energy peak conductance reported here is not sensitive to the position of the Fermi level, varying in magnitude by around 10% (shown in the inset of figure 5) and the variation of the peak position is undetectable within acceptable numerical accuracy. For example, one method to approximately determine the Fermi level is by half-filling the π orbitals via the DOS. The peak conductance so calculated changes from around 5.6 to around 6.1 and the peak position remains unchanged. Doped samples where the Fermi energy does not coincide with the bands-crossing points have very similar optical responses to intrinsic BLG.

In conclusion, we have studied the longitudinal optical conductivity of BLG with the inclusion of all relevant interlayer coupling terms and next nearest neighbor intralayer interactions. The optical conductivity exhibits double peak resonance separated by an amount $2\gamma_1$ and is centered around $\hbar\omega = 2t$. At low energies, the NNN interaction leads to entirely new behavior of the optical conductivity. The results obtained without NNN coupling, however, can be retrieved by appropriate electronic doping. The interplay of the NNN–γ_4 couplings were found to lead to a significant low energy conductance anisotropy which is strongly doping dependent. Finally, the value of the universal conductivity with the most robust formalism used to date has also been determined, and is given by $\sigma_2 = 2\sigma_1$. The applicability of this approximation, however, is restricted to certain energy ranges and is strongly doping dependent. These results will be crucial to the experimental testing of accepted theories on bilayer graphene, and will be useful for potential low energy electronic and photonic applications of bilayer graphene.

Acknowledgments

This work is supported by the Australian Research Council. We also wish to thank Ms Emily Travers for her valuable contribution.

References

[1] Novoselov K S, Geim A K, Morozov S V, Jiang D, Zhang Y, Dubonos S V, Grigorieva I V and Firsov A A 2004 *Science* **306** 666
[2] Geim A K and Novoselov K S 2007 *Nat. Mater.* **6** 183
[3] Novoselov K S, Geim A K, Morozov S V, Jiang D, Katsnelson M I, Grigorieva I V, Dubonos S V and Firsov A A 2005 *Nature* **438** 197
[4] Zhang Y, Tan Y W, Stormer H L and Kim P 2005 *Nature* **438** 201
[5] Berger C *et al* 2006 *Science* **312** 1191
[6] Suzuura H and Ando T 2002 *Phys. Rev. Lett.* **89** 266603
Suzuura H and Ando T 2003 *J. Phys. Soc. Japan* **72** 69
[7] Morozov S V, Novoselov K S, Katsnelson M I, Schedin F, Ponomarenko L A, Jiang D and Geim A K 2006 *Phys. Rev. Lett.* **97** 016801
[8] Khveshchenko D V 2006 *Phys. Rev. Lett.* **97** 036802
[9] Gusynin V P, Sharapov S G and Carbotte J P 2006 *Phys. Rev. Lett.* **96** 256802
[10] Kuzmenko A B, van Heumen E, Carbone F and van der Marel D 2008 *Phys. Rev. Lett.* **100** 117401
[11] Nair R R, Blake P, Grigorenko A N, Novoselov K S, Booth T J, Stauber T, Peres N M R and Geim A K 2008 *Science* **320** 1308
[12] Liu J, Wright A R, Zhang C and Ma Z 2008 *Appl. Phys. Lett.* **93** 041106
[13] Mikhailov S A and Ziegler K 2008 *J. Phys.: Condens. Matter* **20** 384204
[14] Wright A R, Xu X G, Cao J C and Zhang C 2009 *Appl. Phys. Lett.* **95** 072101
[15] Zhang C and Takahashi Y 1993 *J. Phys.: Condens. Matter* **5** 5009
[16] Zhang C 1994 *Phys. Rev.* B **49** 2939
[17] Nilsson J, Castro Neto A H, Guinea F and Peres N M R 2008 *Phys. Rev.* B **78** 045405
[18] McCann E and Falko V I 2006 *Phys. Rev. Lett.* **96** 086805
[19] Nilsson J, Castro Neto A H, Peres N M R and Guinea F 2006 *Phys. Rev.* B **73** 214418
[20] Abergel D S L and Fal'ko V I 2007 *Phys. Rev.* B **75** 155430
[21] Nicol E J and Carbotte J P 2008 *Phys. Rev.* B **77** 155409
[22] Avetisyan A A, Partoens B and Peeters F M 2009 *Phys. Rev.* B **79** 035421
Partoens B and Peeters F M 2006 *Phys. Rev.* B **74** 075404
[23] Li Z Q, Henriksen E A, Jiang Z, Hao Z, Martin M C, Kim P, Stormer H L and Basov D N 2009 *Phys. Rev. Lett.* **102** 037403
[24] Mak K F, Lui C H, Shan J and Heinz1 T F 2009 arXiv:0905.0923
[25] McClure J W 1957 *Phys. Rev.* **108** 612
[26] Slonczewski J C and Weiss P R 1958 *Phys. Rev.* **109** 272
[27] Zhang C, Chen L and Ma Z 2008 *Phys. Rev.* B **77** 241402
[28] Cserti J, Csordas A and David G 2007 *Phys. Rev. Lett.* **99** 066802
[29] Mahan G D 2000 *Many-Particle Physics* (New York: Kluwer Academic)
[30] Stauber T, Peres N M R and Geim A K 2008 *Phys. Rev.* B **78** 085432